First-principles modeling of $Pt/LaAlO_3/SrTiO_3$ capacitors under an external bias potential

Claudio Cazorla[1] and Massimiliano Stengel[1,2,*]
[1]*Institut de Ciència de Materials de Barcelona (ICMAB-CSIC), 08193 Bellaterra, Spain*
[2]*ICREA–Institució Catalana de Recerca i Estudis Avançats, 08010 Barcelona, Spain*
(Received 8 February 2012; published 23 February 2012)

We study the electrical properties of $Pt/LaAlO_3/SrTiO_3$ capacitors under the action of an external bias potential, using first-principles simulations performed at constrained electric displacement field. A complete set of band diagrams, together with the relevant electrical characteristics (capacitance and built-in fields), are determined as a function of $LaAlO_3$ thickness and the applied potential. We find that the internal field in $LaAlO_3$ monotonically decreases with increasing thickness; hence, the occurrence of spontaneous Zener tunneling is ruled out in this system. We discuss the implications of our results in the light of recent experimental observations on biased $LaAlO_3/SrTiO_3$ junctions involving metallic top electrodes.

DOI: 10.1103/PhysRevB.85.075426 PACS number(s): 73.20.−r, 71.15.−m, 71.70.−d

I. INTRODUCTION

In recent years oxide-oxide heterojunctions have generated widespread interest, because of their potential for applications in microelectronics and intriguing fundamental physics. When thin films of polar $LaAlO_3$ (LAO), composed of formally charged $(LaO)^+$ and $(AlO_2)^-$ layers, are stacked on top of the nonpolar (001) surface of $SrTiO_3$ (STO), a two-dimensional (2D) metallic electron gas appears at the interface under suitable experimental conditions.[1] In particular, TiO_2-terminated LAO/STO interfaces are found to undergo an insulating-to-conducting transition (named "electronic reconstruction") when the thickness of the LAO film exceeds three to four layers.[2] Alternatively, 2D metallicity can be switched on and off by applying an external bias potential between the conducting LAO/STO interface and a metallic electrode placed on top of the free LAO surface.[3–8] In the latter setup (i.e., an asymmetric capacitor where the bottom electrode is the 2D electron gas; see Fig. 1) novel striking phenomena have been observed recently, which hold promise for the realization of novel field-effect devices with high operation speed and low power consumption.

First, Singh-Bhalla *et al.*[7] reported a nontrivial dependence of the tunneling current on the LAO thickness, d_{LAO}, with an abrupt increase at $d_{\mathrm{LAO}} = 20$ unit cells. This was ascribed to the presence of a built-in electric field, which would cause Zener breakdown in the LAO film above the aforementioned critical value of d_{LAO}. The electrical response of the tunnel junction also displayed a clear hysteretic behavior as a function of the applied voltage, suggesting interesting opportunities for memory applications. Second, the measured capacitance was found to undergo a remarkable increase at low carrier densities.[8] This enhancement was ascribed to the peculiar electronic properties of the 2D electron gas at the LAO/STO interface, and in particular, to a "negative compressibility" regime. While such a behavior was already known in the context of semiconductor heterojunctions, its unprecedented magnitude (40%) in the LAO/STO system challenges the current theoretical understanding of this effect.

Rationalizing these phenomena in terms of the microscopic properties of the LAO/STO and LAO/electrode junctions is very desirable in sight of future progress. In this context, first-principles electronic structure methods appear ideally suited to describing, with unbiased accuracy, the subtle interplay between carrier confinement, polar distortions, and external electrical perturbations applied to the sample. Indeed the LAO/STO system has been addressed by a large number of *ab initio* studies in the past few years.[9–17] However, studying the phenomena described in Refs. 7 and 8 entails some additional technical challenges, because of the necessity of introducing an external voltage in a complex capacitor system that is overall metallic.

In this paper, we propose an elegant solution to this problem by using recently developed methods[18,19] to perform *ab initio* simulations at constant electric displacement D. In particular, we show that (i) the internal electric field ($\mathcal{E}_{\mathrm{LAO}}$) in a Pt/LAO/STO capacitor is not an intrinsic and fixed quantity, but a function of both applied bias and LAO thickness; (ii) at zero bias, $\mathcal{E}_{\mathrm{LAO}}$ monotonically decreases with film thickness as $\sim 1/d_{\mathrm{LAO}}$, so that no Zener breakdown ever occurs; and (iii) the LAO/STO interface is associated with a finite capacitance, which is predominantly due to band bending effects, and is roughly constant within a wide range of carrier densities. Based on these findings we deduce, entirely *ab initio*, a complete set of band diagrams, and a simple analytical expression for $\mathcal{E}_{\mathrm{LAO}}$ as a function of the relevant parameters. Finally, we discuss the implications of our results for the interpretation of the experimental observations of Refs. 7 and 8.

II. METHODS

A. Constrained-D method

To start with, we are interested in determining the electronic and structural properties of an arbitrarily thick Pt/LAO/STO capacitor subjected to an external bias potential V_{ext}. Instead of working directly at fixed V_{ext}, we use the electric displacement field D as the independent electrical variable; this has clear advantages from the point of view of modeling,[20] as it allows one to break down a layered system into smaller constituents and treat them separately ("locality principle"). Note that working at fixed V or at fixed D yields the exact same information, as V and D are mutually related by a Legendre transformation;[18] for example, one can indifferently define the capacitance density per unit area as $C = dD(V)/dV$ or $C = [dV(D)/dD]^{-1}$. In our case, we shall consider as

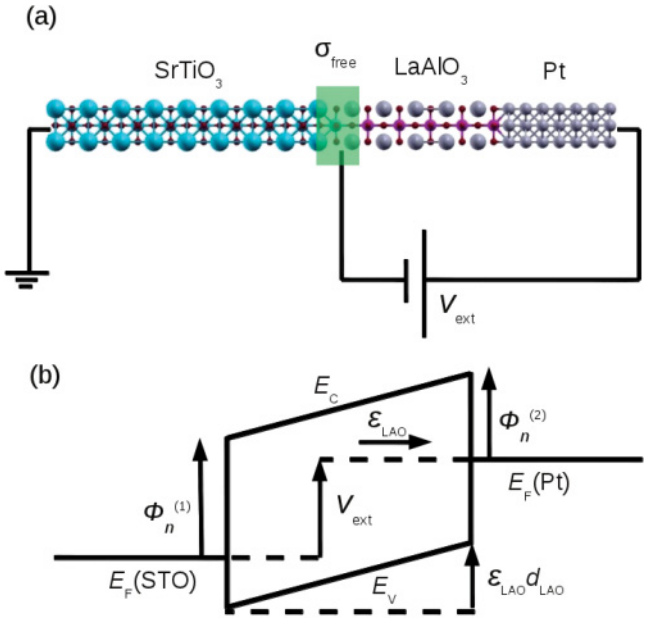

FIG. 1. (Color online) (a) Schematic illustration of the Pt/LAO/STO capacitor: large blue spheres represent Sr atoms; small blue spheres, Ti; red spheres, O; large purple spheres, La; pink spheres, Al; and small purple spheres, Pt. (b) Pt/LAO/STO band diagram: $\phi_n^{(1,2)}$ are the n-type SBH at the LAO/STO and Pt/LAO junctions, $\mathcal{E}_{\rm LAO}$ is the electric field in LAO, $d_{\rm LAO}$ is the thickness of the film, $E_{\rm V}/E_{\rm C}$ are the valence/conduction band edges, $E_{\rm F}$ are the Fermi levels, and $V_{\rm ext}$ is the external bias potential.

our "elementary building blocks" the LAO/STO interface [(1) henceforth], bulk LAO, and the Pt/LAO interface [(2) henceforth]. Thus, following the arguments of Refs. 18 and 21, we decompose the total potential drop $V_{\rm tot}$ across the capacitor into three terms (see Fig. 1),

$$V_{\rm tot}(D,N) = \phi_n^{(1)}(D) - \phi_n^{(2)}(D) + N\,V_{\rm LAO}(D). \qquad (1)$$

Here $V_{\rm LAO} = -\mathcal{E}_{\rm LAO}c_{\rm LAO}$ ($c_{\rm LAO}$ is the out-of-plane lattice parameter) is the potential drop across one unit cell of bulk LAO, N is the number of unit cells, and $\phi_n^{(1,2)}$ are the (D-dependent) n-type Schottky barrier heights (SBH) at the metal/insulator junctions.[18] Note that to obtain the ground state of the system at a given applied potential $V_{\rm ext}$ one simply needs to invert Eq. (1) and solve for $V_{\rm tot}(D,N) = V_{\rm ext}$. This way, the daunting problem of simulating the full Pt/LAO/STO capacitor under an external bias reduces to the more familiar task of calculating SBH at metal/insulator interfaces as a function of D. As we shall explain in the following, it is relatively straightforward to do this with a standard first-principles code, without the need for a specialized finite-field (or even Berry-phase) implementation.

B. Computational details

Our calculations are performed within the local density approximation of density functional theory and the projector augmented wave method,[22] as implemented in the in-house code LAUTREC.[23] We compute the quantities on the right-hand side of Eq. (1) by means of three separate calculations: two interface models within a X/LAO/vacuum slab geometry, where X is the metallic electrode (either Pt or STO), and a periodic bulk LAO model. For the X/LAO interfaces we use stacks of 10/7 (X = Pt) and 12/5 (X = STO) layers, respectively. The in-plane periodicity is set to 1×1 perovskite cells, with the lattice parameter fixed to the theoretical equilibrium value of bulk STO ($a_{\rm STO} = 3.85$ Å). To constrain the electric displacement to a given value we introduce a layer of bound charges Q at the free LAO surface via the virtual crystal approximation.[24] By applying a dipole correction in vacuum, we enforce $D = 0$ outside the free surfaces; then, provided that the surfaces remain locally insulating, we have $D = Q/S$.[19,25] We explore values of D within the range $-0.5e/S \leqslant D_{\rm LAO} \leqslant -0.3e/S$ ($D_{\rm STO}$ is set to zero and $S \equiv a_{\rm STO}^2$).

C. Schottky barrier height estimation

To extract the dependence of the SBH on D, we use computational techniques similar to those of Refs. 25 and 26. In particular, for the estimation of the band offset $\phi_n^{(1,2)}(D)$ we need two independent quantities: the so-called lineup term (an interface property) and the band-structure term (a bulk property).[25] The lineup term relies on the choice of a reference energy in the insulating LAO layer; here we use the La $5s$ semicore energy, which we extract from the layer-resolved density of states of the slab models (see Fig. 2). We define as $E_{5s}^{(1,2)}(D,j)$ the energy location of the La $5s$ peak in the jth LaO layer of the (1) or (2) system, referred to as the Fermi level of the corresponding metallic electrode (either Pt or STO). In the case of zero internal field, $E_{5s}^{(1,2)}(D,j)$ converges to a constant value for layers j lying sufficiently far away from the interface or the surface (typically two to three unit cells), and the definition of the lineup term is straightforward. Conversely, when the electric field in LAO is nonzero (see Fig. 3), E_{5s} has a linear dependence on the layer index. In particular, deep enough in the film, the variation of E_{5s} between two consecutive cells corresponds precisely to the bulk internal field at the same value of D,

$$E_{5s}^{(1,2)}(D,j+1) - E_{5s}^{(1,2)}(D,j) = V_{\rm LAO}(D). \qquad (2)$$

Therefore, once $V_{\rm LAO}(D)$ is known (from the bulk calculations), we can define an *extrapolated* reference energy (see Fig. 3),

$$E_{\rm ref}^{(1,2)}(D,j) = k(D) + j\,V_{\rm LAO}(D), \qquad (3)$$

where the constant $k(D)$ is chosen in such a way that $E_{\rm ref}(D,j) = E_{5s}(D,j)$ far from the interface. Then, we define the lineup term as

$$\phi_{\rm ref}^{(1,2)}(D) = E_{\rm ref}^{(1,2)}\left(D, j_{\rm I}^{(1,2)}\right), \qquad (4)$$

where $j_{\rm I}^{(1,2)}$ indicates the interface plane location; here we assume $j_{\rm I}^{(1)} = 3/4$ and $j_{\rm I}^{(2)} = 1/4$ (see Fig. 3). Finally, to obtain the n-type SBH $\phi_n^{(1,2)}(D)$ we just need to add to $\phi_{\rm ref}^{(1,2)}(D)$ the D-dependent band-structure term [we calculate it in the bulk, as the difference between the La($5s$) level and the conduction band minimum] $E_{\rm CBM}(D)$,

$$\phi_n^{(1,2)}(D) = \phi_{\rm ref}^{(1,2)}(D) + E_{\rm CBM}(D). \qquad (5)$$

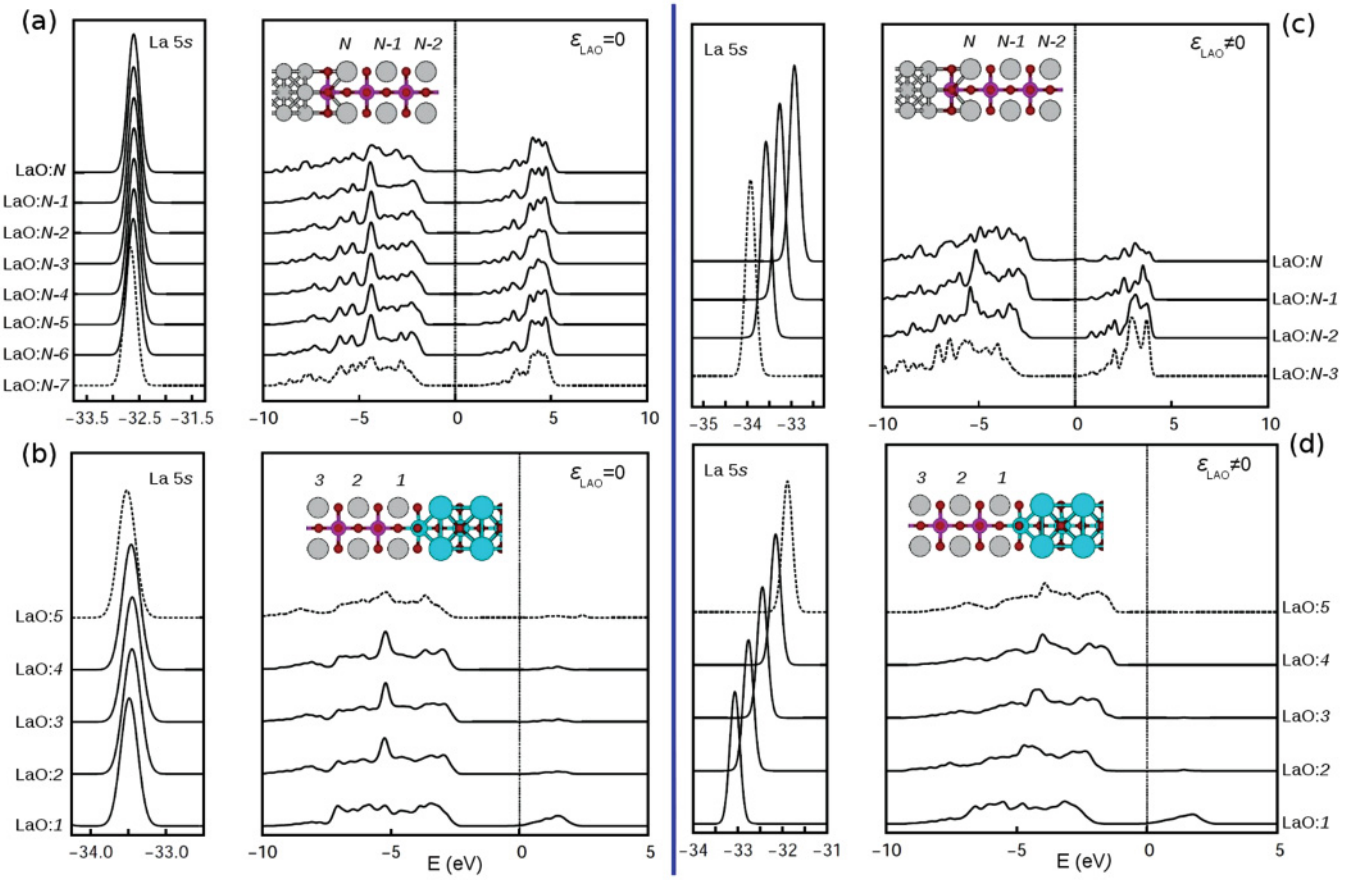

FIG. 2. (Color online) Projected density of states (PDOS) of the inequivalent LaO layers in the Pt/$LaAlO_3$/$SrTiO_3$ capacitor (shifted along the y axis in order to facilitate the visualization and expressed in arbitrary units). [(a),(c)] PDOS are obtained in the Pt/$LaAlO_3$ slab system at zero and finite LAO internal field, respectively. [(b),(d)] Plots are analogous to (a) and (c) but obtained in the $LaAlO_3$/$SrTiO_3$ system. PDOS calculated in the layers closest to vacuum are shown with dashed lines. Layer ordering is explicitly shown along the y axis and all Fermi energy levels have been shifted to zero. The atomic color code is the same as that explained in Fig. 1.

III. RESULTS AND DISCUSSION

Our results for $\phi_n^{(1,2)}(D)$ and $V_{\rm LAO}(D)$ are shown in Figs. 4(a) and 4(b). We find that $\phi_n^{(1,2)}(D)$ behave linearly within the whole studied range. Consequently, the *total* potential drop due to both interfaces can be expressed as $V_{\rm I}(D) = V_{\rm I}^0 + C_{\rm I}^{-1}(D + e/2S)$, where $V_{\rm I}^0$ is the total interface potential drop at $D = -e/2S$ and the coefficient $C_{\rm I}^{-1}$ physically corresponds to the overall inverse interface capacitance density.[18,21] Considering the potential drop in bulk LAO also to be linear in D [see Fig. 4(b)], i.e., $V_{\rm LAO}(D) \approx C_b^{-1}(D + e/2S)$, we obtain a simple yet very accurate analytical expression for the electric displacement field in LAO,

$$D(V_{\rm ext}, N) + \frac{e}{2S} \approx \frac{V_{\rm ext} - V_{\rm I}^0}{NC_b^{-1} + C_{\rm I}^{-1}}, \qquad (6)$$

where $C_b^{-1} = 1.36$ m^2/F, $V_{\rm I}^0 = -0.83$ V, and $C_{\rm I}^{-1} = 1.57$ m^2/F ($S \equiv a_{\rm STO}^2$). The inverse bulk LAO capacitance density C_b^{-1} is directly related to the static dielectric constant of LAO, $\bar{\epsilon}_{\rm LAO}$, via $C_b^{-1} = c_{\rm LAO}/(\epsilon_0 \bar{\epsilon}_{\rm LAO})$; in our computational model we have $\bar{\epsilon}_{\rm LAO} = 31$. For a given value of D, we compute the corresponding electric field using $\mathcal{E}_{\rm LAO} = (D + e/2S)/\bar{\epsilon}_{\rm LAO}$. [In the "exact" treatment we replace the average $\bar{\epsilon}_{\rm LAO}$ with the calculated $\epsilon_{\rm LAO}(D)$; see the inset of Fig. 4(c)]. Our results for $\mathcal{E}_{\rm LAO}(V_{\rm ext}, N)$ are shown in Fig. 4(c). It is worth noting that the outcomes of Eqs. (1) [exact, considering nonlinearities in $V_{\rm LAO}(D)$] and (6) (approximate) are in excellent agreement. In both cases we find that $\mathcal{E}_{\rm LAO}(V_{\rm ext}, N)$ monotonically decreases with the inverse of LAO thickness, independently of the applied bias potential.

These results have important implications concerning the interpretation of the experiments reported in Ref. 7. First, no intrinsic *built-in* LAO electric field exists in the short-circuited Pt/LAO/STO capacitor system, contrary to the assumptions of Singh-Bhalla *et al.*[7] Second, and most importantly, the uniform decrease of $\mathcal{E}_{\rm LAO}(V_{\rm ext}, N)$ with LAO thickness in practice rules out the hypothesis of Zener breakdown, which was used in Ref. 7 to explain the abrupt increase of the tunneling current at $N \sim 20$. Indeed, as $\mathcal{E}_{\rm LAO}(V_{\rm ext}, N)$ decreases with increasing N, Zener tunneling becomes increasingly less likely in thicker films—note that in our model the LAO valence band *never* goes above the STO Fermi level unless a strong external potential $V_{\rm ext} \sim 1.8$–1.9 eV is applied. An alternative interpretation of the aforementioned tunneling experiments rests on the results of Ref. 27. Precisely at a thickness of ~20 unit cells, Cancellieri *et al.* reported the onset of in-plane strain relaxation in the LAO overlayer. Such relaxation processes are

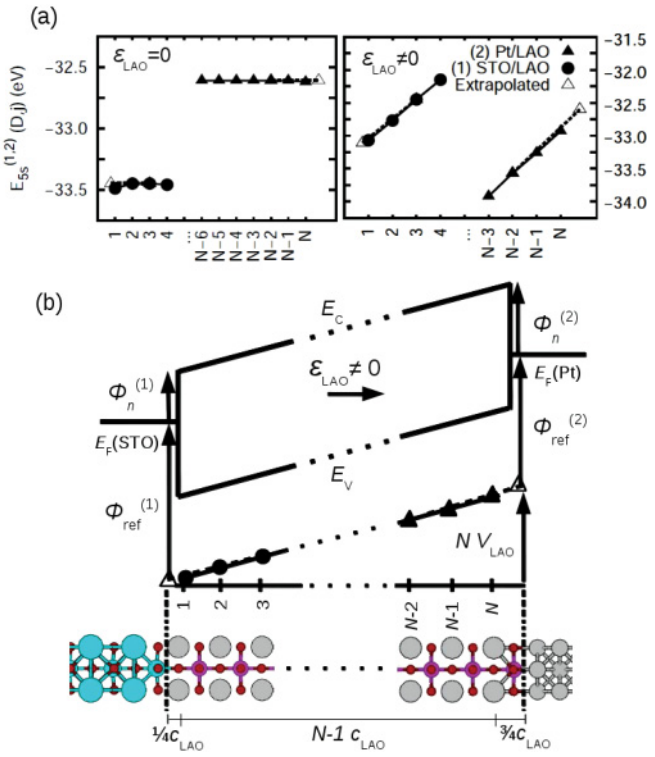

FIG. 3. (Color online) (a) Layer-resolved La 5*s* semicore energies $E_{5s}^{(1,2)}$ obtained at $D=-0.5e/S$ (left) and $-0.3e/S$ (right). Triangles represent the extrapolated values at the interfaces $\phi_{\rm ref}^{(1,2)}$. (b) Sketch of the Pt/LAO/STO band diagram and details of the extrapolation scheme (see text).

known to induce defects (e.g., cracks, or misfit dislocations) in the LAO film.[27,28] It is not unreasonable to think that these defects might constitute preferential paths for electron or hole conduction; also, these defect-mediated conduction processes might explain the hysteretic behavior of the electrical diagrams of Ref. 7. (The authors invoked the presence of switchable dipoles at the LAO/STO interface, which appears puzzling as neither LAO nor STO are ferroelectric.)

Finally, we shall comment on the microscopic mechanisms that lead to the calculated interface properties. The total interface capacitance density can be expressed as the sum of two contributions,

$$C_{\rm I}^{-1}=\frac{d}{dD}\left(\phi_n^{(1)}-\phi_n^{(2)}\right)=\frac{1}{C^{(1)}}+\frac{1}{C^{(2)}}, \qquad (7)$$

each due to a different interface. The variation of $\phi_n^{(2)}(D)$ with D is very small (see Fig. 4); this means that the Pt electrode behaves ideally ("perfect" screening[25]), i.e., $1/C^{(2)}\sim 0$, and therefore we restrict the following analysis to the LAO/STO junction. Specifically, we shall consider the effects of band bending on $1/C^{(1)}$, i.e., the D-dependent interfacial potential drop that occurs in STO due to the presence of the confined charge carriers.[29] To estimate the band-bending contribution $\phi_{\rm STO}(D)$, we have employed the tight-binding (TB) model[30] introduced in Ref. 19. We define $\phi_{\rm STO}(D)$ as the value of the electrostatic potential in STO at the interfacial Ti site, referred to as the Fermi level of the confined electron gas, at a given D [see Figs. 5(a) and 5(c)]. Our results show that $\phi_{\rm STO}(D)$ behaves linearly within a wide range of values [Fig. 5(d)]. The

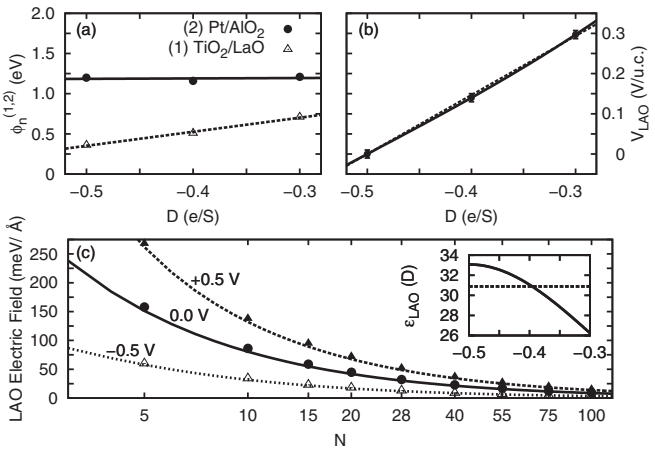

FIG. 4. (a) Calculated *n*-SBH as a function of D. The curves represent the linear fits $\phi_n^{(1)}(D)=0.35+1.62(D+e/2S)$ and $\phi_n^{(2)}(D)=1.18+0.05(D+e/2S)$ (in units of V). (b) Calculated potential drop per unit cell of bulk LAO; $V_{\rm LAO}(D)=1.27(D+e/2S)+2.24(D+e/2S)^3$ (solid line) and $V_{\rm LAO}(D)=1.36(D+e/2S)$ (dashed line). (c) $\mathcal{E}_{\rm LAO}$ as a function of the number of LAO layers and bias potential $-0.5\leqslant V_{\rm ext}\leqslant 0.5$ V. The x axis is in logarithmic scale. Symbols and lines represent results obtained with Eqs. (1) and (6), respectively. Inset: Static dielectric constant of bulk LAO as a function of DS/e (solid curve) and the corresponding averaged value $\bar{\epsilon}_{\rm LAO}$ (dashed line).

band-bending contribution to $1/C^{(1)}$ corresponds to the slope of the linear fit, which amounts to 1.03 m^2/F. This contribution constitutes a significant fraction (approximately two-thirds) of $1/C^{(1)}$. The remainder of $1/C^{(1)}$ is likely to be caused by

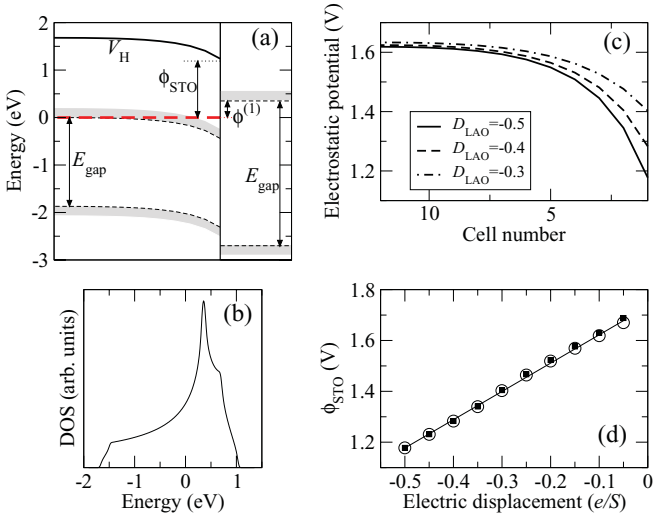

FIG. 5. (Color online) (a) Mesoscopic band diagram of the LAO/STO junction. The electrostatic potential in STO, $V_{\rm H}$ (thick solid curve), the conduction and valence band edges (shaded dashed curves), and the Fermi level (thick dashed line) are shown. (b) Ti t_{2g} density of states of our TB model ($V_{\rm H}$ is constant and set to zero). (c) $V_{\rm H}$ as calculated with the TB model (Fermi levels are shifted to zero). (d) Electrostatic potential at the interfacial Ti site as a function of D. Empty circles (filled squares) are calculated for a 12- (24-) layer STO slab and the solid line represents a linear fit to the data.

other effects that typically occur at oxide-oxide interfaces, e.g., intrinsic dielectric "dead layers."[31,32] As these appear to be of secondary importance here, we have not pursued this analysis further.

The above results are timely for the interpretation of recent capacitance measurements of thin-film electrode/LAO/STO heterostructures.[8] In the regime of large carrier densities, Li *et al*. measured a dielectric constant of the LAO film of $\epsilon_{\mathrm{LAO}} \sim 18$, which is significantly smaller than the typical value reported for LAO single crystals ($\epsilon_{\mathrm{LAO}} = 25$–$30$). In light of the results of our study, it is not unreasonable to think that interfacial effects, and not only the film quality, might contribute to the small measured value of ϵ_{LAO}. To verify whether this might be the case, we estimated the total averaged dielectric constant (i.e., considering both interface and bulk capacitances), $\overline{\epsilon}_{\mathrm{tot}}$, of our Pt/LAO/STO nanocapacitor as

$$\frac{1}{\overline{\epsilon}_{\mathrm{tot}}} = \frac{1}{\overline{\epsilon}_{\mathrm{LAO}}}\left(1 + \frac{C_b}{NC^{(1)}}\right). \tag{8}$$

By using the $\overline{\epsilon}_{\mathrm{LAO}}$, C_b, and $1/C^{(1)}$ (=1.62 m^2/F) values calculated in this work, and a LAO film thickness of 10–12 cells, we obtain $\overline{\epsilon}_{\mathrm{tot}} \sim 28$, i.e., only a 10% reduction compared to the bulk value of $\overline{\epsilon}_{\mathrm{LAO}}$. The discrepancy between this result and measurements may be related to the quality of the LAO film, as proposed in Ref. 8, and/or to the fact that in their experiments Li *et al*. used YBCO electrodes instead of the Pt ones considered here.

With regard to this latter hypothesis, note that oxide electrodes typically tend to be associated with a significantly smaller interface capacitance than elemental metal electrodes such as Pt or Au.[31] Thus, it is not unreasonable to think that YBCO electrodes might have a much stronger effect on $\overline{\epsilon}_{\mathrm{tot}}$ than the Pt electrodes used in this work (recall that $1/C^{(2)}$ essentially vanishes in the present Pt/LAO case), and this should be taken into account when comparing our data to those of Ref. 8. Note that, in order to verify this hypothesis, there is no need to repeat the calculations for the whole capacitor (i.e., including the LAO/STO interface and LAO bulk). One only needs to calculate the properties of the YBCO/LAO interface, extract the relevant parameters (band offset at zero field and interface capacitance $C^{(2)}$), and plug them into Eq. (6) [or in Eq. (1) in case there were significant nonlinearities in $\phi^{(2)}(D)$].

As a last remark, we would like to briefly discuss whether our computational strategy might be appropriate to address the large capacitance enhancements that were reported in Ref. 8. In fact, the sheet carrier densities considered in this work ($2.0 \leqslant \sigma_{\mathrm{free}} \leqslant 3.4 \times 10^{14}$ e/cm^2, where $\sigma_{\mathrm{free}} = D_{\mathrm{LAO}} - D_{\mathrm{STO}}$[19]) are very large compared to those measured by Li *et al*. (0.1–10.0×10^{12} e/cm^2), so our results cannot be straightforwardly extrapolated to the experimentally relevant regime. A possible strategy to overcome this limitation would be to perform similar calculations at a substantially lower carrier density, e.g., by applying a back-gating voltage to the STO substrate. In this case, however, one would also need to assess whether the local density approximation is able to capture the negative compressibility of the 2D electron gas, or whether one needs a more sophisticated description of electron correlation. Another important question to be carefully considered is whether the decomposition of Eq. (1) is appropriate on a general basis. In other words, can we always consider the electrodes as macroscopically separated entities, or do we also need to take into account *direct* interactions? Indeed, some authors recently claimed that negative capacitance effects would emerge from direct couplings between the individual electrons of the two-dimensional electron gas and their image charge at the metal electrode.[33–35] Clearly, Eq. (1) breaks down in such a scenario, and would need to be complemented with additional physical ingredients. We believe that the above open questions constitute exciting avenues for future theoretical investigations, and we hope that our work will stimulate further studies along these directions.

IV. CONCLUSIONS

In summary, we have studied the electrical properties of metal/LAO/STO capacitors fully from first principles, determining a complete physical picture of the band offsets and internal fields. Our results and methodologies open new avenues in the first-principles study of functional oxide heterostructures, and provide useful guidelines for the interpretation of the available experimental data on this system.

ACKNOWLEDGMENTS

This work was supported by MICINN-Spain (Grants No. MAT2010-18113 and No. CSD2007-00041), ICREA, and the EC-FP7 project OxIDES (Grant No. CP-FP 228989-2). Computing time was kindly provided by BSC-RES and CESGA.

*mstengel@icmab.es

[1] A. Ohtomo and H. Y. Wang, Nature (London) **427**, 423 (2004).
[2] S. Thiel, G. Hammerl, A. Schmehl, C. W. Schneider, and J. Mannhart, Science **313**, 1942 (2006).
[3] C. Cen, S. Thiel, G. Hammerl, C. W. Schneider, K. E. Andersen, C. S. Hellberg, J. Mannhart, and J. Levy, Nat. Mater. **7**, 298 (2008).
[4] W. M. Lü, X. Wang, Z. Q. Liu, S. Dhar, A. Annadi, K. Gopinadhan, A. Roy Barman, H. B. Su, T. Venkatesan, and Ariando, Appl. Phys. Lett. **99**, 172103 (2011).
[5] R. Jany *et al*., Appl. Phys. Lett. **96**, 183504 (2010).
[6] G. Cheng *et al*., Nat. Nanotechnol. **6**, 343 (2011).
[7] G. Singh-Bhalla, C. Bell, J. Ravichandran, W. Siemons, Y. Hikita, S. Salahuddin, A. F. Hebard, H. Y. Hwang, and R. Ramesh, Nat. Phys. **7**, 80 (2011).
[8] L. Li, C. Richter, S. Paetel, T. Kopp, J. Mannhart, and R. C. Ashoori, Science **332**, 825 (2011).
[9] R. Pentcheva and W. E. Pickett, Phys. Rev. Lett. **102**, 107602 (2009).
[10] K. Janicka, J. P. Velev, and E. Y. Tsymbal, Phys. Rev. Lett. **102**, 106803 (2009).
[11] P. Delugas, A. Filippetti, V. Fiorentini, D. I. Bilc, D. Fontaine, and P. Ghosez, Phys. Rev. Lett. **106**, 166807 (2011).

[12]Z. S. Popovic, S. Satpathy, and R. M. Martin, Phys. Rev. Lett. **101**, 256801 (2008).
[13]S. A. Chambers, L. Qiao, T. C. Droubay, T. C. Kaspar, B. W. Arey, and P. V. Sushko, Phys. Rev. Lett. **107**, 206802 (2011).
[14]L. Qiao, T. C. Droubay, T. C. Kaspar, P. V. Sushko, and S. A. Chambers, Surf. Sci. **605**, 1381 (2011).
[15]H. Chen, A. M. Kolpak, and S. Ismail-Beigi, Adv. Mater. **22**, 2881 (2010).
[16]W.-J. Son, E. Cho, B. Lee, J. Lee, and S. Han, Phys. Rev. B **79**, 245411 (2009).
[17]N. C. Bristowe, P. B. Littlewood, and E. Artacho, Phys. Rev. B **83**, 205405 (2011).
[18]M. Stengel, N. A. Spaldin, and D. Vanderbilt, Nat. Phys. **5**, 304 (2009).
[19]M. Stengel, Phys. Rev. Lett. **106**, 136803 (2011).
[20]X. Wu, M. Stengel, K. M. Rabe, and D. Vanderbilt, Phys. Rev. Lett. **101**, 087601 (2008).
[21]M. Stengel, D. Vanderbilt, and N. A. Spaldin, Nat. Mater. **8**, 392 (2009).
[22]P. E. Blöchl, Phys. Rev. B **50**, 17953 (1994).
[23]We used a plane-wave energy cutoff of 40 Ry and a $6 \times 6 \times 1$ Monkhorst-Pack **k**-point grid for Brillouin zone sampling. In the geometry optimizations, atomic forces along the out-of-plane direction were imposed to be smaller than 5 meV/Å.
[24]The additional charge density is introduced by substituting a cation at the ferroelectric surface by a fictitious cation of different formal valence. As we are interested in exploring intermediate values of D, we generated fictitious pseudopotentials that reproduced fractional nuclear charges.
[25]M. Stengel, P. Aguado-Puente, N. A. Spaldin, and J. Junquera, Phys. Rev. B **83**, 235112 (2011).
[26]M. Stengel, D. Vanderbilt, and N. A. Spaldin, Phys. Rev. B **80**, 224110 (2009).
[27]C. Cancellieri *et al*., Phys. Rev. Lett. **107**, 056102 (2011).
[28]Y. Wang, S. G. Kim, and I-W. Chen, Acta Mater. **56**, 5312 (2008).
[29]K. Yoshimatsu, R. Yasuhara, H. Kumigashira, and M. Oshima, Phys. Rev. Lett. **101**, 026802 (2008).
[30]This is based on an electronic t_{2g} Hamiltonian describing the hoppings between Ti-centered orbitals, wherein the electrical boundary conditions are defined by the electric displacement field in LAO.
[31]M. Stengel and N. A. Spaldin, Nature (London) **443**, 679 (2006).
[32]O. Copie *et al*., Phys. Rev. Lett. **102**, 216804 (2009).
[33]M. S. Bello, E. I. Levin, B. I. Shkolovskii, and A. L. Efros, Sov. Phys. JETP **53**, 822 (1981).
[34]B. Skinner and B. I. Shklovskii, Phys. Rev. B **82**, 155111 (2010).
[35]B. Skinner and M. M. Fogler, Phys. Rev. B **82**, 201306(R) (2010).